An Efficient Two-Polymer Binder for High-Performance Silicon Nanoparticle-Based Lithium-Ion Batteries: A Systematic Case Study with Commercial Polyacrylic Acid and Polyvinyl Butyral Polymers

JES Focus Issue of Selected Papers from IMLB 2018

An Efficient Two-Polymer Binder for High-Performance Silicon Nanoparticle-Based Lithium-Ion Batteries: A Systematic Case Study with Commercial Polyacrylic Acid and Polyvinyl Butyral Polymers

Anna Urbanski,[1,z] Ahmad Omar,[2] Jing Guo,[2] Andreas Janke,[1] Uta Reuter,[1] Mikhail Malanin,[1] Florian Schmidt,[1] Dieter Jehnichen,[1] Matthias Holzschuh,[1] Frank Simon,[1] Klaus-Jochen Eichhorn,[1] Lars Giebeler,[2] and Petra Uhlmann[1,3,z]

[1]*Leibniz-Institut für Polymerforschung (IPF) Dresden e.V., Institut für Physikalische Chemie and Physik der Polymere, 01069 Dresden, Germany*
[2]*Leibniz-Institute for Solid State and Material Research (IFW) Dresden e.V., Institute for Complex Materials, 01069 Dresden, Germany*
[3]*Department of Chemistry, University of Nebraska-Lincoln, Lincoln, Nebraska 68588, USA*

Silicon is one of the most promising anode materials for high energy density lithium ion batteries (LIBs) due to its high theoretical capacity and natural abundance. Unfortunately, significant challenges arise due to the large volume change of silicon upon lithiation/delithiation which inhibit its broad commercialization. An advanced binder can, in principle, reversibly buffer the volume change, and maintain strong adhesion toward various components as well as the current collector. In this work, we present the first report on the applicability of polyvinyl butyral (PVB) polymer as a binder component for silicon nanoparticles-based LIBs. Characteristic binder properties of commercial PVB and polyacrylic acid (PAA) polymers are compared. The work focuses on polymer mixtures of PVB polymers with PAA, for an improved binder composition which incorporates their individual advantages. Different ratios of polymers are systematically studied to understand the effect of particular polymer chains, functional groups and mass fractions, on the electrochemical performance. We demonstrate a high-performance polymer mixture which exhibits good binder-particle interaction and strong adhesion to Cu-foil. PAA/PVB-based electrode with a Si loading of ~1 mg/cm^2 tested between 0.01 and 1.2 V vs. Li/Li$^+$ demonstrate specific capacities as high as 2170 mAh/g after the first hundred cycles.
 [DOI: 10.1149/2.0371903jes]

Manuscript submitted October 26, 2018; revised manuscript received December 11, 2018. Published January 2, 2019. *This paper is part of the JES Focus Issue of Selected Papers from IMLB 2018.*

Lithium ion batteries (LIBs) have found prominence as the most promising energy storage systems for almost all portable electronic devices, electric vehicles (EVs) and stationary energy storage due to their high energy density and high operating voltage as compared to other secondary batteries.[1,2] Since their introduction in 1991, the energy densities of commercialized LIBs have steadily increased up to four times.[3] However, the extractable capacity in the conventional systems based on a graphite anode and phosphate or lithium oxide cathodes is close to the theoretical limit,[4] for example, in graphitic anodes, six carbon atoms can store only one lithium ion (LiC_6) corresponding to a theoretical gravimetric capacity of 372 mAh/g.

In order to surpass that limit, there are ongoing efforts to explore higher capacity anode materials. Silicon is one of the most attractive ones since it has an extremely high theoretical capacity of 3579 mAh/g (as per lithiation to $Li_{15}Si_4$ at room temperature) and a low discharge/lithiation voltage around 0.4 V vs. Li/Li$^+$, in addition to being naturally abundant and environmentally benign.[5–7] Unfortunately, during the lithiation process of Si, an immense undesirable volume change of about 300% takes place. The large volume change during each cycle is the primary reason for the chronic capacity fading during cycling which represents the main obstacle in silicon's practical implementation.[2,8] The large volume expansion (during lithiation) and contraction (during delithiation) results in pulverization and cracking of the electrode, which also causes the loss of the electrical contact between Si particles and the conducting framework. Furthermore, this repeated volume change promotes side reactions of the Si surface with the electrolyte leading to an unstable and thick solid electrolyte interphase (SEI) layer. Over multiple cycles this results in a continuous loss of the active material, irreversible consumption of Li ions and, as a consequence, increase of the internal resistance, which contributes strongly toward a quick failure.[6,9]

A large body of work exists toward addressing these problems of silicon, and nanostructuring of Si has been found to considerably buffer the large volume change,[2] thereby minimizing the mechanical degradation both at the particle and electrode level and substantially improving the battery performance. Significant progress has been made to develop various Si nanoarchitectures such as nanoparticles (Si-NPs), nanowires, nanotubes, thin films, and nanoporous silicon, to name a few.[6,10–12] Additionally, novel active materials involving carbon-coating, core-shell frameworks and hierarchical structures involving Si have been reported to show further enhanced electrochemical behavior.[10,11]

However, despite the various elegant approaches and their brilliant performances, most of these nanomaterials are synthesized by complex and multistep processes to achieve specific structures, resulting in high costs and lower scalability for potential industrial applications. Moreover, the low electrical conductivity of silicon means that a relatively large amount (15–30 wt%) of conductive carbon is needed to make sufficient electric contacts across the electrode. Therefore, it becomes clear that in order to hold together these nanostructured materials and the conductive additives, a backbone of polymer binder becomes an inevitable and a pivotal component.[13–15]

An ideal polymer binder acts as a glue to homogeneously bind all parts of the electrode slurry together as well as strongly adheres to the current collector, and thus, it serves to maintain the integrity of electrodes. In the specific case of silicon, a good binder should possess mechanical robustness to reversibly buffer the significant volume fluctuations continuously over long term cycling such that it can also be used with a wide range of silicon morphologies, especially commercially viable ones. Also, the binder should not only be flexible and have low swelling with the electrolyte but at the same time should

[z]E-mail: urbanski@ipfdd.de; uhlmannp@ipfdd.de

support electrical and Li-ion conductivity. Moreover, with regards to the technical requirements, it should be easily producible in large quantities, inexpensive and compatible with a standard manufacturing method (i.e. slurry casting).

Conventional polyvinylidene difluoride (PVdF) binders, commonly used in graphite electrodes, have been proven to be not suitable for Si-based electrodes due to their highly non-polar structure which leads to weak Van der Waals interactions with the electrode components, as well as low elastic modulus.[14] Synthetic[16–18] and natural polymers[19] such as carboxymethyl cellulose (CMC) and its mixture with styrene-butadiene rubber (SBR),[20] polyimide,[21] alginates[22] etc. are also actively studied as potential binders but their lack of optimal solvents for slurry preparation is a drawback. Various new polymer binders have been reported, e.g., cross-linked polymers, catechol-conjugated polymer, "host-guest", conductive polymers, etc.[14,23] However, here as well many of them require complicated in-house synthesis[24] for which commercial viability of their production is unknown.

To date, polyacrylic acid (PAA) is the most broadly used binder for Si anodes.[25] In addition to being soluble in ethanol for facile electrode preparation, PAA has many advantages such as mechanical stiffness and minimal swelling in the electrolyte solvent, thus preserving sufficient mechanical properties in the presence of the electrolyte. The COOH functional groups can interact well with the native oxide layer of silicon via H-bonding but cannot fully accommodate the sustained large volume changes in the case of silicon, leading to cracking of the coating with cycling.[26] Moreover, it does not adhere strongly to the current collector due to its highly polar structure and an increase in the mass loading results in an easy delamination from the commonly used Cu foil.[27]

Herein we present the first report on the use of polyvinyl butyral (PVB) as a binder for lithium battery electrodes. A copolymer poly(vinyl butyral-*co*-vinyl alcohol-*co*-vinyl acetate) is known for its strong binding, adhesion, toughness and flexibility.[28,29] It is already used in many industrial coatings and membranes, especially as the main component of polymer films on laminated safety glass for various applications.[29,30] The underlying reason for the aforementioned use is the presence of alcohol groups which leads to a formation of a reversible but dense network of weak hydrogen bonds with the silanol groups of the glass. Thus the chemical structure of the PVB copolymer shows potential advantages toward application for silicon anodes: OH-groups for adhesion to the native oxide layer (SiO_x), non-polar butyral groups for good adhesion to conductive carbon additives as well as for electrolyte uptake leading to a better Li-ion conductivity.[31]

However, since acetal (butyral) groups prevail by the weight percentage in the PVB it is likely that the polymer may soften in the electrolyte and thus lose its mechanical stiffness.[31] Nonetheless, the advantages offered by PVB nicely complement the advantages of PAA. Therefore, the present study at first assesses PVB polymers as individual binders for Si-NPs'-based electrodes for LIBs and then focuses on PAA/PVB mixtures as two-polymer binder systems. In the present work, two commercial PVB polymers with different molecular weights were chosen. We studied the individual polymer properties of both PVBs as well as commercial PAA. Such PAA/PVB systems should allow good interaction between the binder and the native oxide layer of silicon, while maintaining sufficient mechanical robustness. The composition of the polymer mixtures was chosen with regard to polymer chemical parameters as molar ratio and ratio of COOH and OH groups with the aim to get insights into rational material and component design in the field of batteries. The electrochemical performance of the electrodes is discussed taking into account material scientific issues of the used binder systems.

Experimental

Materials.—Silicon nanoparticles (Silicon, 98+%, mean diameter: 30–50 nm, laser synthesized) were obtained as a powder from US Research Nanomaterials (USA). Conductive carbon black (CB) powder (TIMCAL Super C65) and copper foil (9 mm thick) were purchased from MTI Corporation (USA). The low molecular weight poly(vinyl butyral-*co*-vinyl alcohol-*co*-vinyl acetate) sample with M_w = 60 000 g/mole (PVB60) was received from Kuraray Europe (Germany) under the specification Mowital B60T. The high molecular PVB sample with $M_w \sim$ 170 000-240 000 g/mole (PVB210), poly(acrylic acid) with $M_w \sim$ 450 000 g/mole (PAA450), the electrolyte mixture composed of 1.0 M lithium hexafluorophosphate ($LiPF_6$) salt in ethylene carbonate (EC) and dimethyl carbonate (DMC), EC/DMC = 1:1 (v/v), battery grade, were all purchased from Sigma Aldrich (Germany). Electrolyte solvents (EC and DMC) were purchased from Acros Organics (Germany). Analytical data on PVB polymers is given in Table I.

Table I. Composition of PVB polymer samples given by the supplier.

PVB specification	PVB60	PVB210
wt% of vinyl alcohol	24–27	17.5–20
wt% of vinyl butyral	72	80
wt% of acetate	1–4	0–2.5

Silicon nanoparticle characterization.—Shape and crystallinity of the Si-NPs were examined with a transmission electron microscope (TEM, Libra200, Carl Zeiss Microscopy GmbH, Germany) operated at 200 kV. Figure S1a-c of the Supplementary Material shows that the average size of Si-NPs is in the range of 30–50 nm as indicated by the producer, with a small fraction of smaller (~10 nm) and bigger (~75 nm) particles. The high magnification TEM-micrograph in Figure S1b indicates that the particles are crystalline with a distinguishable oxide layer with thickness between 2 nm and 5 nm. The selected area electron diffraction image in Figure S1c fits well to the crystal structure of Si (*Fd*-3*m*, space group no. 227).

The crystalline purity of the as-received Si-NPs was analyzed by X-ray diffraction (XRD) experiments. Measurements were executed at room temperature by means of the 2-circle diffractometer XRD 3003 T/T (GE Sensing & Inspection Technologies/Seifert-FPM, Germany). The X-ray diffraction pattern (Figure S2) and details on data evaluation are given in the Supplementary Material.

X-ray photoemission spectroscopy (XPS) measurements were conducted to study the silicon surface. The XPS study on Si-NPs was carried out by means of an Axis Ultra photoelectron spectrometer (Kratos Analytical, Manchester, UK). The spectrometer was equipped with a monochromatic Al Kα ($h \cdot \nu$ = 1486.6 eV) X-ray source of 300 W at 15 kV. Quantitative elemental compositions were determined from peak areas using experimentally determined sensitivity factors and the spectrometer transmission function. The spectrum background was subtracted according to Shirley.[32] After subtraction of the Shirley background, the Si 2p core-level spectra were fitted with Gaussian−Lorentzian line shapes using Kratos spectra deconvolution software. The Si-NPs exhibit a major component at a binding energy of 99.6 eV, which is associated with elemental silicon. An additional component at approximately 103 eV indicates that roughly 14 wt% of the Si atoms are oxidized. The details on data evaluation and XPS spectra (Figure S3) are given in the Supplementary Material.

Preparation of thin PAA and PVB films.—For the swelling experiments and determination of mechanical properties by atomic force microscopy (AFM), PAA and PVB thin films were prepared by spin-coating technique from 0.5 wt% polymer solutions. Absolute ethanol was used as the solvent for PAA450 and absolute THF for PVB60 and PVB210. For spin-coating the Si (100) wafers, purchased from Si-Mat (Germany), were cut into 1 × 2 cm pieces, treated with absolute ethanol in an ultrasonic bath three times for 10 minutes each and activated in an oxygen plasma chamber for 1 min at 100 W. Directly after activation of the Si-wafers, polymer solutions were filtered using a syringe filter (PTFE, pore size 0.2 μm) and deposited by spin coating (n = 2500 rpm, a = 1000 rpm s^{-1}, V = 150 μL, t_{spin} = 10 s).

Table II. Summary of prepared PAA/PVB mixtures.

Composition	PAA450/PVB60			PAA450/PVB210		
prefix*	Mass ratio	Molar ratio	$n_{(COOH)}$:$n_{(OH)}$	Mass ratio	Molar ratio	$n_{(COOH)}$:$n_{(OH)}$
blue-	8:1	1:1	19:1	2:1	1:1	6.5:1
orange-	1:2.4	1:18	1:1	1:3.3	1:7	1:1
black-	2:1	1:4	5:1	8:1	4:1	26:1

*prefix indicates the corresponding color in the electrochemical data for ease of understanding (see Figures 2–5).

Polymer films had thickness in the range of 27–47 nm. As-prepared polymer films were dried under vacuum at 80°C for 2 hours.

Determination of the Young's modulus and swelling ratio of PAA and PVB thin films by atomic force microscope (AFM).—Nanoindentation studies were done with AFM by tip indentation techniques[33] on the thin polymer films prepared by spin-coating. Studies were performed on a Dimension FastScan AFM (Bruker-Nano, USA). Force-distance data were collected using FastScan-B cantilevers (Bruker-Nano, USA). The spring constant in the range of 1 N/m to 3 N/m was estimated by the thermal noise method, the tip radius was 5 nm nominally. Force-volume measurements in a 2 × 2 array with a distance of 200 nm between the points were analyzed by the NanoScope Analysis software (Bruker-Nano, USA) to obtain Young's modulus using the Hertz model.

In order to determine the thickness of the PAA and PVB films, a deep scratch by a razor blade on the polymer film reaching the substrate, i.e. Si-wafer, was done at first. The mean step height of three scratches at different locations was measured by AFM. The same measuring procedure was used to define the thickness of the polymer film in the "wet" state in order to define the swelling ratio.

Both nanoindentation measurements and determination of the film thickness were performed on samples in both "dry" and "wet" state, where the latter one refers to the one achieved by immersing the spin-coated polymer film into 2 mL of electrolyte mixture EC/DMC = 1:1 (v/v) for at least 5 minutes and then taken out.

Determination of the adhesion force of PAA and PVB to the Si-surface by AFM.—The Si wafers were cut into 1 × 1 cm pieces and treated with absolute ethanol in an ultrasonic bath three times for 10 minutes each before use. After cleaning, the Si wafers were incubated in a highly diluted polymer solution overnight, i.e. 0.5 mg mL^{-1} of PAA450, PVB60 or PVB210 ethanol solutions. Next day the pre-treated Si wafers were taken out of the polymer solutions, rinsed with ethanol and left to dry at room temperature. Such washing procedure guarantees to wash off all the polymer which is not adhered to the surface of the Si wafer and enables to perform the following AFM pulling experiment on a single-molecular level.[34]

Pulling measurements were carried out using a Dimension ICON AFM (Bruker-Nano, USA). Sharpened triangular silicon nitride cantilevers OTR-8 (Bruker-Nano, USA) were used throughout the study, with a nominal spring constant of 0.57 N/m. All AFM force experiments were conducted in ethanol at room temperature with a tip velocity of 1 μm sec^{-1} without delay of a tip on the Si surface. The force curves were taken at three different locations on the Si wafer, at each location 9 curves were measured in a 3 × 3 array with distances of 200 nm between the points. Force curves were analyzed by the NanoScope Analysis software v1.9 (Bruker-Nano, USA). The adhesion force was measured after baseline correction.

Electrode fabrication.—Typically, 180 mg of Si-NPs' powder, 60 mg of CB powder and 3 mL of polymer solution in ethanol with a concentration of 20 mg/mL were ball-milled in a 10 mL stainless steel beaker with 15 stainless steel balls (Ø: 3 mm) using a mixer mill MM 400 (Retsch, Germany) at 25 Hz for 2 hours. Thus, the composition of all electrode slurries was 60 wt% of Si-NPs, 20 wt% of CB and 20 wt% of the polymer binder. Despite three electrodes with PAA450, PVB210, and PVB60 polymers used as mono-polymer binders, six additional electrodes with PAA/PVB binder mixtures had been prepared. The composition of PAA/PVB mixtures defines the electrode name using three prefixes: blue-, orange- and black-. The mass ratio and the molar ratio of two polymers in each mixture, as well as the ratio of COOH groups of PAA to OH groups of PVB, are given in Table II. In the discussion part *Polymer blends as electrode binders*, classification is discussed in detail. The following example should shed light on the preparation of PAA/PVB mixtures for the slurry: In order to prepare the blue-PAA450/PVB60 electrode, 2.67 mL of PAA450 polymer solution with a concentration of 20 mg/mL had been mixed with 0.33 mL of PVB60 polymer solution of the same concentration, i.e. 20 mg/mL and added to the ball milling beaker. After the slurry was homogenized in the ball-mill it was immediately casted on Cu foil using a Zehntner doctor blade (ZUA 2000, Zehntner, Switzerland) with a clearance of 250 μm, dried in the air for 30 minutes and under vacuum at 100°C for 4 hours and subsequently at 150°C for 1 hour. Thermal gravimetric analysis (TGA) of PAA450, PVB60 and PVB210 confirmed that the polymers are stable within the drying temperature range (See Supplemental Material, Table S1).

Electrode characterization.—The electrode density was defined by first taking a number of circular discs with a diameter of 10 mm from the main electrode film with an area of ∼65 cm^2. Mass and thickness of each disc were determined using a microbalance (MT5, Mettler Toledo GmbH, Switzerland) and micrometer (MDC-25MX, Mitutoyo Corporation, Japan). The averaged mass and thickness of Cu foil were determined in the same manner. Although the thickness of the Cu-foil is given by the supplier as 9 μm, from numerous measurements and SEM-micrographs its thickness was determined to be 10.3 μm. The areal loading of the electrode coatings was determined to be in the range of 1.5–1.8 mg/cm^2 and densities were calculated to be in the range of 0.59–0.65 g/cm^3 depending on the exact binder composition (Table III). The slight difference in the porosity originates from the viscosity of the electrode slurry, which is in turn dependent on the polymer binder composition.

Table III. Characteristics of electrodes prepared with different polymers/polymer-mixtures used as the binder.

Electrode name	Avg. mass loading, (mg/cm^2)	Avg. thickness (μm)	Avg. density (g/cm^3)
PAA450	1.56	25.6	0.609
PVB210	1.49	23.1	0.645
PVB60	1.58	24.2	0.653
blue-PAA450/PVB210	1.52	25.05	0.607
black-PAA450/PVB210	1.56	26.2	0.595
orange-PAA450/PVB210	1.64	26.6	0.616
blue-PAA450/PVB60	1.65	26.8	0.615
black-PAA450/PVB60	1.76	30.1	0.585
orange-PAA450/PVB60	1.51	24.4	0.619

Scanning electron microscopy (SEM).—Morphology and microstructure of the electrodes were examined using a scanning electron microscope (SEM, NEON40, Carl Zeiss Microscopy GmbH, Germany), operated at the accelerating voltage of 3 kV. Figures S4-S12 give an overview on SEM-micrographs of each electrode's surface and cross-section. The names of electrodes are given as in Table III. Before the post-mortem analysis of the electrodes, a sputtering with 3.5 nm of platinum (Sputter Coater SCD500, Leica Microsystems GmbH, Germany) was applied to reduce the charging.

Ultramicrotome.—The electrode cross sections were prepared at room temperature using an ultramicrotome EM UC6/FC6 (Leica, Austria) fitted with a diamond knife (Diatome, Switzerland). The cutting speed was 2 mm/s.

Electrochemical testing.—The electrochemical properties of electrodes were investigated using Swagelok cells (Swagelok, Germany). A lithium metal disc with a diameter of 10 mm was used as the counter and reference electrode and 1 M $LiPF_6$ in EC/DMC = 1:1 (v/v) with 10 wt% of fluoroethylene carbonate (FEC) was used as the electrolyte. The volume of the electrolyte per Swagelok cell was 250 μL. Each working Si-electrode was punched from the main film into circular chips with a diameter of 10 mm. Two chips of Whatman membranes (Fiberglass, Grade GF/D, Whatman, USA) with a diameter of 10.5 mm were used as separators. The cells were assembled in a glove box filled with argon ($H_2O \leq 1$ ppm, $O_2 \leq 1$ ppm). Galvanostatic charge-discharge cycling was performed with the BST8-MA Multichannel Battery Analyser (MTI Corporation, USA) within a voltage range of 1.2−0.01 V using the constant current mode.

Sample preparation for post-mortem analysis by SEM.—At first 4 electrode chips of the same electrode composition were assembled in a glove box using Swagelok cells and set to cycle galvanostatically within a voltage range of 1.2−0.01 V using a constant current of 0.25 $A/g_{(Si)}$. The use of Swagelok cells is particularly suitable for the post mortem analysis of the electrodes. The advantage compared to coin cells is that there is no need to use a high pressure during decrimping. Swagelok cells can be easily opened, i.e. unscrewed, and thus cause less damages to the cycled material. After the desired number of cycles were finished, the cells were disassembled within next 10 hours in a glove box. The withdrawn electrode chips were subsequently washed by the electrolyte solvent EC/DMC = 1:1 (v/v) three times and at the end rinsed by DMC. The final washing with DMC is done in order to avoid the EC left on the electrode surface since EC is solid at room temperature. The electrodes were left to dry in a glove box overnight after washing. Due to strong delamination from the Cu-foil of certain electrode chips, they were required to be embedded in an instant adhesive (Superflex Gel, UHU GmbH, Germany) before performing the cutting procedure with the ultramicrotome.

The information about precise electrode mass loading is extremely important for this experiment in order to determine the electrode expansion as realistic as possible. The aim is to compare the electrode thickness considering a defined cycling history with its pristine thickness, i.e. the state before cycling. It means that after defining the thickness of the cycled electrode from SEM images, the degree of its expansion has to be calculated not using the averaged thickness of the electrode given in Table III but rather calculating the thickness from the actual mass loading and the density of the particular electrode chip used. The following example should shed light on this issue more clearly. In the case of the blue-PAA450/PVB60 system, the electrode chip used for 10 cycles had a mass loading of 1.56 g/cm^2. Its initial thickness, calculated based on its density of 0.615 g/cm^3, is 25.3 μm instead of 26.8 μm given in Table III as an averaged value. The thickness of the electrode after 10 cycles defined from SEM is 35.88 μm. For defining the degree of expansion, we divide 35.88 μm over 25.34 μm and get ∼142% expansion. Without this correction the averaged value would be ∼134%.

Determination of PAA-PVB interactions by attenuated total reflection-Fourier transform infrared spectroscopy (ATR-FTIR).—The prepared electrode coatings are not suitable for the FTIR analysis with respect to PAA/PVB interactions because of high concentrations of carbon black in the system under consideration, which results either in a striking decrease of the spectrum quality or in an inability to obtain a reliable spectrum even when using a germanium-ATR-crystal. Therefore in order to determine whether PAA and PVB undergo a chemical reaction (e.g. esterification), or whether any intermolecular interactions occur (e.g. hydrogen bonding), polymer films were prepared via a simple blend membrane preparation method. The PAA/PVB polymer solutions in ethanol with the mass ratios of PAA450 to PVB60 or to PVB210 (Table II) with a total polymer concentration of 30 mg/mL were first stirred overnight. Next day, 10 mL of the polymer solution was casted onto a glass Petri dish, and was allowed to evaporate at room temperature. It was dried next day under vacuum at 100°C for 4 hours and subsequently at 150°C for 1 hour. The drying conditions were exactly the same as for the slurry casted electrodes. The as-prepared polymer films (Figure S13) were used for FTIR characterization.

ATR-FTIR spectra of the polymer powders (PAA450, PVB60 and PVB210) and free standing PAA/PVB film mixtures were measured using the FTIR spectrometer Vertex 80v (Bruker, Germany) equipped with both a mercury–cadmium–telluride (MCT)-detector (InfraRed Associates Inc., USA) and single reflection diamond Golden Gate ATR-unit (Specac, UK). The spectral range was 4000–600 cm^{-1} with a spectral resolution of 4 cm^{-1}. 100 scans were co-added to every ATR-spectrum. As part of the post-processing of ATR-spectra, a spectral baseline correction was performed in addition to a normalization of the mixture spectra using the stretching vibration band of methylene group (at 2937 cm^{-1})[35] as an internal Reference 36.

Bulk scale peeling experiments.—In order to determine the peel strength of the electrode specimens, 7 mm wide and 25 mm long electrode strips were punched out of the main electrode coating and a 7 × 7 mm electrode area was attached to a Scotch Transparent Tape. The samples were measured by means of high-precision Digital Force Gauge (FH2, Sauter GmbH, Germany) in the 180° setup. The measurements were conducted with a constant displacement rate of 50 μm/s, the applied load was continuously monitored and force-displacement plots were generated.

Results and Discussion

Although PAA, and to some extent PVB, as a polymer has been studied in detail with regard to various mechanical and physical properties, there are differences in polymer production and suppliers, characterization techniques and measuring conditions, which makes it rather difficult to compare one sample to the other.

Therefore, we first performed an extensive characterization of pristine PAA and PVB polymers under similar conditions. This allowed us to easily compare their mechanical and physical properties, as well as to establish a baseline for the polymer mixtures. In order to minimize variance, commercially available individual polymers from the same batch were chosen. For the purpose of this study, in addition to PAA, we have taken two PVB polymers with different molecular weights and fractions of various functional groups. The details are summarized in Table I. Polymer films were prepared on Si (100) substrate using spin-coating, which were then used for measurements of swellability, Young's modulus and adhesion force.

Swellability of PAA- and PVB-films in the electrolyte solvent.—The polymer-electrolyte interaction was characterized by the swelling behavior of the polymers using AFM in a mixture of EC/DMC = 1:1 (v/v), which is the most common solvent system used for silicon anodes. The swellability of a polymer film is defined as the ratio of the thickness of the film immersed in electrolyte solvent to the thickness of the pristine dry film. Figure 1a shows the swelling behavior of the three polymers. PAA450 has a lower swelling ratio than the two PVB

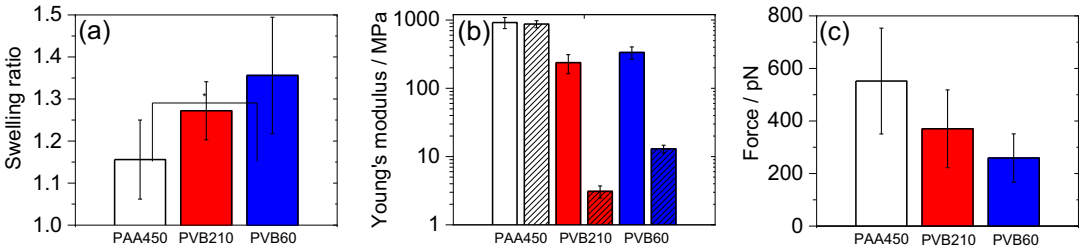

Figure 1. Characterization of PAA- and PVB polymers: (a) Swelling ratios (normalized thickness) of PAA- and PVB-films in EC/DMC = 1:1 (v/v), as measured by AFM; (b) Young's modulus of PAA- and PVB-films measured by AFM. Hatched bars and empty bars correspond to measurements made in EC/DMC = 1:1 (v/v) and in air, respectively; (c) Interaction forces of PAA and PVB polymers with silicon substrate as obtained from AFM pulling experiments.

polymers, which qualitatively indicates a lower polymer-solvent intermolecular interaction of polar PAA polymer with non-polar electrolyte solvents. It has been reported[17] that thin PAA-films showed negligibly small swellability of ∼1% in contrast to ∼15% found in our measurements. The preparation method of the polymer films (spin-coating in our case vs. dip-coating by Magasinski et al.[17]) influences the packing of polymer chains on the silicon substrate and its final thickness (>50 nm vs. few microns, respectively). Moreover, the used analytical techniques (AFM vs. ellipsometry, respectively) and the compositions of the electrolyte solvent (1:1 (v/v) mixture of EC:DMC vs. DMC, respectively) also have an impact on the results of the swelling behavior. As mentioned earlier, the difference in the experimental setup and measurement conditions among various studies makes it difficult to easily compare results.

The interaction of PVB with the electrolyte solvent mixture is higher than the one of PAA due to the predominant presence of non-polar butyral functional groups in the PVB structure. Comparing the two PVB polymers, the swellability of PVB60 sample is slightly stronger than that of PVB210, which can be attributed to a lower packing density of shorter PVB60 polymer chains on the Si wafer and in turn a higher penetration by the carbonate molecules of the solvents. The stronger swelling of PVB implies that during electrochemical cycling of the Li-Si cells, PVB may be more strongly involved into the SEI formation process than PAA since many works have shown that a polymer binder influences the SEI composition and also that there is a strong effect of a larger polymer-electrolyte intermolecular interaction.[37,38] On the other hand, a stronger electrolyte uptake of PVB may improve the electrolyte wettability of the electrode. For example, in the work by Lian et al., PVB had been used as the main component of the gel polymer electrolyte[31] and in the study by Sun et al., it was proposed that the presence of O-heteroatoms in the binder for Si-anodes, similar as in the PVB structure, can improve the lithium-ion transfer within the binder molecules.[39] Thus, we presume that PVB may also contribute to a better Li^+ conductivity at the interface between PVB and Si-NPs.

Mechanical stiffness of PAA- and PVB-films.—Nano-indentation measurements were performed by AFM to characterize the mechanical properties of the polymers (Young's modulus). The stiffness of PAA and PVB in the dry state indicates that PAA450 is a much stiffer polymer than PVB (Figure 1b). Specifically, Young's moduli of three polymers were measured to be 920 MPa for PAA450, 237 MPa for PVB210 and 335 MPa for PVB60, which is consistent with published data.[40,41,17] Mechanical properties of both PVB polymers change significantly when exposed to a carbonate-based solvent, which is in accordance with the swellability measurements. Young's modulus decreases by ∼90%, i.e. to 13 MPa and 3 MPa for PVB60 and PVB210, respectively, whereas in the case of PAA450, it changes only by ∼5%, i.e. from 920 MPa in the air to 874 MPa in the electrolyte solvent (Figure 1b).

These results suggest that PVB should behave as an easily deformable binder in the electrolyte solution, with small resistance to elastic deformation. Since Si undergoes a significantly large volume expansion during lithiation (up to ∼300%) the binder may become incapable of keeping Si particles in contact during subsequent volume contraction. Such characteristics of the binder are not desirable as they may lead to a capacity fade during cycling due to contact loss.[42,13] The results are similar to PVdF, a binder known to provide an unstable performance to Si electrodes, which was reported to have its stiffness decreased by ∼98% from a value of ∼600 MPa after immersion in the electrolyte solvent.[22,17] However, unlike PVdF, which is only capable of weak Van der Waals interactions with all constituents of the electrode (Si-NPs, CB and Cu-foil), OH-functional groups of PVB should allow a better adhesion toward the surface of Si particles via hydrogen bonding and also via Van der Waals interactions of butyral moieties to the conductive carbon additive.

Adhesion of PAA and PVB to Si.—In order to evaluate the polymer/Si interaction, AFM pulling tests were conducted on Si substrates (Figure 1c). The average peeling force values obtained are 550 pN for PAA450, 370 pN for PVB210 and 260 pN for PVB60. The better adhesion of PAA to Si is due to the COOH functional groups which can interact well with the oxidized Si surfaces via H-bonding. On the other hand, the lower adhesion forces in case of PVB are explained by the predominant presence of butyral groups (Table I). It should be noted that the observed force magnitude for PAA/Si peeling test is higher than the one reported earlier.[43,34] Therefore, we use these results primarily to understand a qualitative trend of adhesion forces toward silicon for the PAA and PVB polymers, and, as will be discussed later, utilize it to better interpret the electrochemical performance.

Polymer blends as electrode binders.—Subsequent to characterization of the individual polymers, pure PAA and both PVBs as well as polymer mixtures of PAA/PVB were prepared and used as binders for electrode preparation with commercial Si-NPs. Specific care was taken in choosing the ratio of PAA/PVB polymers in the mixtures especially since we have two different types of PVB polymers with different fractions of functional groups.

There are two main scenarios when a mixture of PAA/PVB polymer chains can form an efficient network and have an optimal impact on the electrode performance: (i) with the equal amount of PAA and PVB chains, i.e. equal molar ratio of polymers; or (ii) with the equal amount of functional groups, i.e. the number of carboxylic groups $n_{(COOH)}$ of PAA is equal to the number of hydroxyl groups $n_{(OH)}$ of PVB, which can interact with each other either via H-bonding or forming an ester covalent bond. Therefore, one set of mixtures was prepared with equal mole ratio of PAA/PVB (prefix: blue) and one with equal functional groups ($n_{(COOH)}$:$n_{(OH)}$ = 1:1; prefix: orange). Considering the averaged M_w of each polymer and corresponding weight percent of OH groups in the PVB samples (Table I), we calculated corresponding mass ratios for each PAA/PVB composition which are summarized in Table II. An additional set of mixtures was prepared with the same mass ratio of PAA/PVB mixtures (prefix: black) for better comparison, since mechanical properties may be determined by the more prominent polymer by mass. For clarity, the black-PAA450/PVB60 mixture has the same mass ratio as the blue-PAA450/PVB210, and the black-PAA450/PVB210 has the same mass ratio as the blue-PAA450/PVB60 (Table II). The prefix

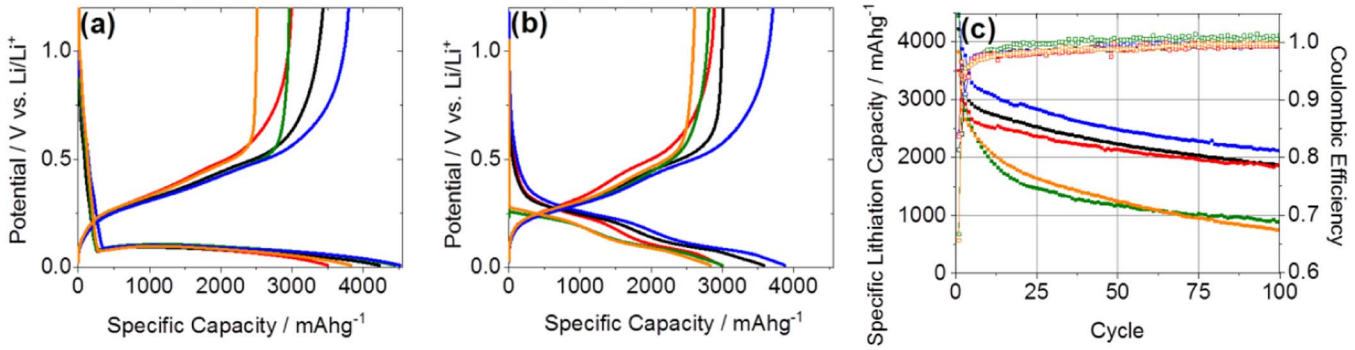

Figure 2. (a) Lithiation/delithiation profiles of the 1st and (b) of the 2nd cycle and (c) specific lithiation capacity and Coulombic efficiency of electrodes cycled at a current density of 0.25 A/$g_{(Si)}$ within 0.01 and 1.2 V vs. Li/Li^+ with following binders: (red symbols) PAA450, (green symbols) PVB60, (blue symbols) blue-PAA450/PVB60, (orange symbols) orange-PAA450/PVB60, (black symbols) black-PAA450/PVB60 binder compositions (Table II).

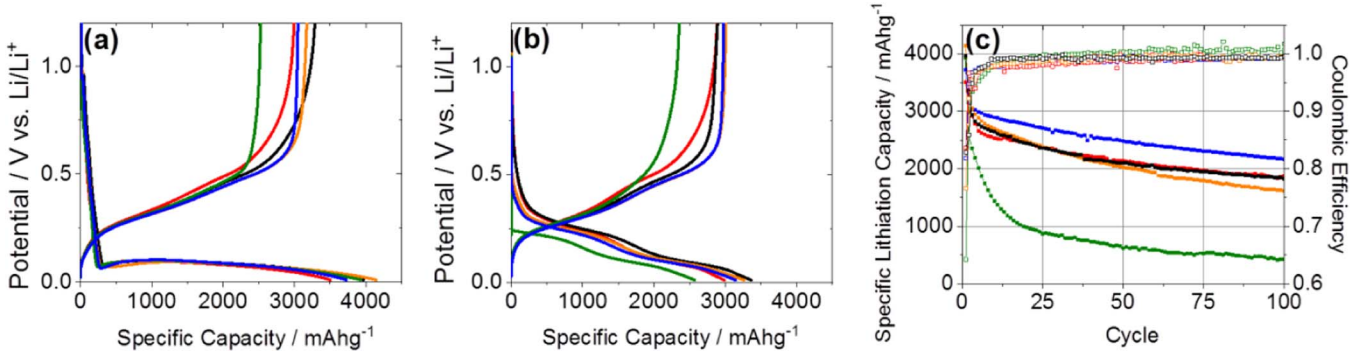

Figure 3. (a) Lithiation/delithiation profiles of the 1st and (b) of the 2nd cycle and (c) specific lithiation capacity and Coulombic efficiency of electrodes cycled at a current density of 0.25 A/$g_{(Si)}$ within 0.01 and 1.2 V vs. Li/Li^+ with following binders: (red symbols) PAA450, (green symbols) PVB210, (blue symbols) blue-PAA450/PVB210, (orange symbols) orange-PAA450/PVB210, (black symbols) black-PAA450/PVB210 binder compositions (Table II).

indicates the corresponding color in the electrochemical data for ease of understanding (see Figures 2–5). Therefore a total of six PAA/PVB polymer mixtures were strategically considered.

Correspondingly, nine sets of electrodes were prepared using PAA450, PVB210, PVB60 or one of six PAA/PVB polymer mixtures as binder. The electrodes were prepared by slurry casting containing 60 wt% Si-NPs, 20 wt% binder and 20 wt% CB with ethanol as solvent. The measured average thickness of the electrode sheet and the corresponding average mass loading were used to define the electrode densities. The density values for all nine electrode sheets lay in the narrow range of 0.59–0.65 g/cm^3 as shown in Table III (see Experimental Section).

Detailed characterization of the electrodes was done in order to study the electrode morphology. SEM images of all nine electrode surfaces and cross-sections show a uniform structure and smooth surface with small pores (<100 nm) visible between Si-nanoparticles (Figures S4-S12). SEM images at high magnifications of 10 kX and 40 kX show that the porosity of all electrodes is visually comparable, although it was not measured separately. Given the theoretical density of CB (160 g/cm^3), Si (2.3 g/cm^3) and used polymers (~1 g/cm^3), we can understand that the remaining pore volume in each electrode is at least three times the volume of Si-NPs[22] indicating sufficient space in the electrodes for the volume change of Si under lithiation/delithiation.

In order to examine the homogeneity of mixed components in the electrodes, scanning electron microscopy (SEM) images using back-scattered electron detector (BSE) images were taken. The overview on SEM micrographs are presented in Figures S14-S15 (see Supplementary Material) and representative examples at a higher magnification

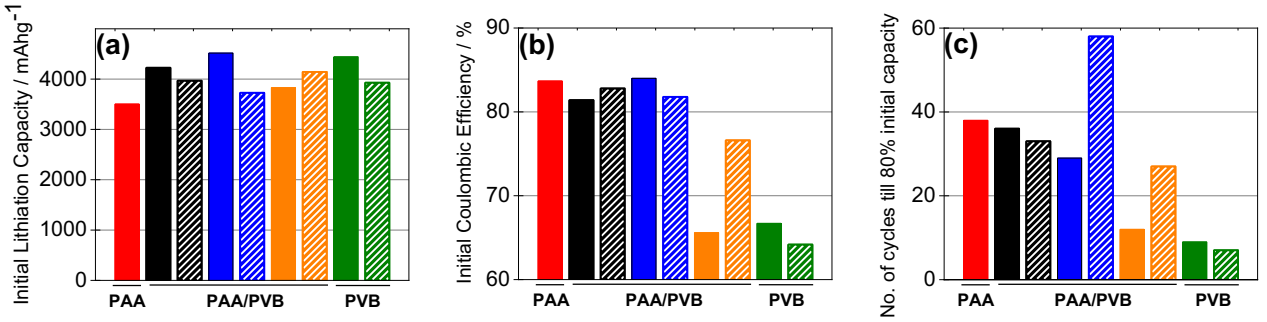

Figure 4. (a) Comparison of the initial specific lithiation capacities, (b) of the initial Coulombic efficiency and (c) of number of cycles till 80 % of the 4th lithiation capacity for electrodes with (red) PAA450-, (green) PVB and (blue, orange, green) PAA/PVB mixtures. Hatched bars correspond to the respective PVB210 and PAA450/PVB210 mixtures; solid filled bars correspond to PVB60 and PAA450/PVB60 mixtures (Table II).

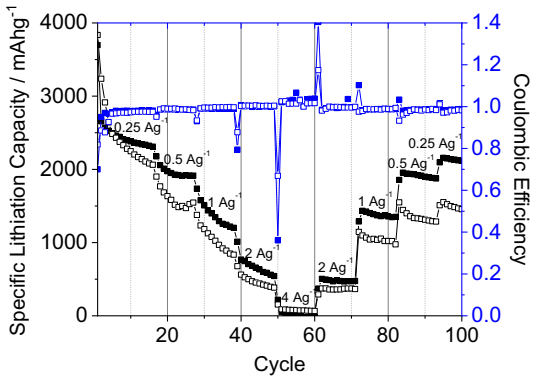

Figure 5. Specific lithiation capacity (black symbols) and Coulombic efficiency (blue symbols) of electrodes cycled at different current density within 0.01 and 1.2 V vs. Li/Li$^+$ with blue-PAA450/PVB210 (full symbols) and blue-PAA450/PVB60 (empty symbols) compositions.

in Figure S16. Both PVB-based electrodes show an excellent mixing of Si-NPs and conductive additives, whereas the PAA-based electrode displays micron-scale non-uniformity, with regions of predominately CB (dark component) interspersed within regions of predominately Si-NPs (light component) (Figure S16). A bad homogeneity of PAA-based electrodes was reported earlier by Higgins et al.[44] The presence of segregations in the electrode, which is undesirable, means that Si-NPs may not be in close proximity to the conductive additive. Thus the electrochemical reaction with electrons and the lithium ion transfer may not be complete, which may in turn lead to lower capacity.

We believe that such a difference in mixing is closely related to the chemical structure of the polymer backbone. PVB has non-polar butyral moieties that are compatible with the non-polar surface of CB. In contrast, due to the highly polar nature of PAA, it mixes worse with CB additives and tends to form segregations of Si-NPs, due to a stronger adhesion of PAA to the Si-NP surface (Figure 1c). Therefore, it is understandable that for those PAA/PVB electrodes, where PAA is predominant by weight in the PAA/PVB mixtures (Table II), the segregation of components is more severe (Figures S14-S15).

Electrochemical performance.—Electrochemical characterization was performed to assess the individual PVB polymers as binders in comparison to PAA, and also study the influence of PAA/PVB compositions on the resulting electrochemical performance. Testing was carried out using a Swagelok cell setup in a half-cell configuration with lithium foil as both a reference and a counter electrode. Galvanostatic cycling was performed to nearly 100% depth-of-discharge (to 0.01 V–1.2V vs. Li/Li$^+$) and neither the insertion capacity nor the lower potential threshold was limited. Also, the current density was set to 0.25 A/$g_{(Si)}$, i.e ∼0.07 C-rate or ∼0.25 mA/cm^2, without initial formation cycles.

The resulting voltage profiles of the first lithiation/delithiation cycle are shown in Figure 2a and Figure 3a. In general, all Si-based electrodes show a long plateau at <0.10 V vs. Li/Li$^+$ during the first lithiation. At this stage, crystalline Si nanoparticles gradually transform into an amorphous Li_xSi phase ($x = 3.4\pm0.2$) with no abrupt structural changes visible, as indicated by the absence of multiple voltage plateaus.[5,45] At about 0.4 V vs. Li/Li$^+$ the curvature of the Li extraction curve changes from negative to positive, which indicates formation of an *a*-Li_xSi phase and eventual formation of *a*-Si. The second and subsequent Li-insertion curves also exhibit a gradual voltage change (Figures 2b, 3b) with no clear plateaus which is related to the absence of crystalline Si after the first lithiation.[46]

The specific lithiation/delithiation capacities of each electrode were calculated based on the mass of the active material, i.e. mass of Si. The effect of the binder composition on the initial lithiation capacity is displayed in Figure 2a and in Figure 3a and summarized in Figure 4a: comparing both PAA/PVB series, the electrode with PAA binder exhibits the lowest initial lithiation capacity (see Table S2). The low initial lithiation capacity is attributed to the poor homogeneity of PAA-based electrodes as demonstrated by the distribution of Si and CB particles in the electrodes by SEM imaging (Figures S14-S16). The segregation of Si leads to a lack of effective electron pathways causing lower activation of Si. However, once PVB is present as a part of the binder blend, it facilitates the mixing of Si and CB particles and eventually more efficient lithiation of the active material. Thus, Si anodes with either PVB or with a mixture of PAA/PVB demonstrate higher initial capacities.

Observed first lithiation capacities are higher than the theoretical capacity of 3579 mAh/g for Si.[5] This is not unusual and has been reported in many previous works.[22,47,44] Since in general the measured capacity is calculated as a multiplication of time and current used for the galvanostatic cycling, a large amount of SEI formation takes place during the first lithiation which also consumes Li-ions in side reactions and on the surface of Si, thus leading to a higher initial capacity than the theoretical one. However, the initial Coulombic efficiency (CE) of 85.5% for the PAA-based electrode is much higher than those for electrodes with pure PVB60 or PVB210 (Figure 4b, Table S2), where only ∼65 % of Li ions return to the reference electrode. In turn, CE is significantly improved once PVB is mixed with PAA and, increases with the increasing mass fraction of PAA in the PAA/PVB blends (Table II). This indicates a larger irreversible consumption of Li-ions with higher mass fractions of PVB in the polymer mixtures. Due to the soft nature of PVB, unlike PAA, it is unable to accommodate well the volume expansion of Si during lithiation/delithiation and thus can promote this undesirable process. On one hand, these effects can be explained by a stronger interaction of PVB with the electrolyte solvent (discussed in the previous subchapter, Figure 1) which may lead to a stronger SEI formation and side reactions. On the other hand, these results may imply that once PAA is present, less SEI is formed due to its lower polymer/electrolyte solvent interaction (Figures 1a and 1b) and a higher adhesion strength toward the surface of Si-NPs (Figure 1c). A detailed study about the influence of PVB on SEI formation and related issues, such as changes in the internal resistance, will be a focus of our future work.

The specific lithiation capacity from the cycling data given in Figures 2c and 3c shows that for both PAA/PVB series, the electrodes with equal molar ratios of PAA to PVB polymers (blue-PAA/PVB compositions) show the best performance and the highest specific capacity. Although the improvement in comparison to the second best performing electrodes, which is either the electrode with PAA450 or with the black-PAA/PVB compositions, is only ∼260–320 mAh/g which may not seem substantial with respect to the overall specific capacity, it is comparable to the theoretical capacity of graphite anodes (372 mAh/g).

The strategy for different mixtures of PAA and two PVB polymers was based on the same molar ratio of PAA and PVB chains (blue-PAA/PVB compositions), same ratio of functional groups (orange-PAA/PVB compositions) and comparable mass ratio between the mixtures of PVB polymers (black-PAA/PVB compositions). Both blends with the blue composition show the best performance among all compositions. It is to be noted that although the molar ratio of PAA and PVB are equal in both blue mixtures, the mass ratio (PAA:PVB) in blue-PAA450/PVB60 is 8:1, whereas in blue-PAA450/PVB210 composition it is 2:1. For the orange compositions (with equal ratio of COOH- and OH-groups), the orange-PAA450/PVB210 electrode has a capacity twice as high after 100 cycles as the orange-PAA450/PVB60 electrode (Figures 2c and 3c). The two compositions are rather similar with respect to mass ratio (1:2.4 vs. 1:3.3) but the molar ratios between PAA and PVB polymers are remarkably different for the two: 1:18 for PAA450/PVB60 and 1:7 for PAA450/PVB210 (Table II).

These observations indicate that both (i) the molar ratio of PAA and PVB polymer chains and (ii) the ratio of COOH and OH groups closer to equal are important for the improvement of the capacity fade. Thus formation of a denser polymer net, to what these two conditions can

contribute, is the most beneficial feature toward improved electrode performance.

We have also tried to compare the capacity fade among the electrodes by looking at its cycling life. A cell is considered to be at the end of its cycle life when its discharge capacity sinks below a critical threshold, which is usually 80 % of its initial lithiation capacity.[48,49] Therefore, for a better comparison of the electrodes' ability for capacity retention we defined such a state of a capacity fade as the number of cycles with a capacity higher than 80% of the forth lithiation capacity.[48,49] Among the two compositions with equal molar ratios showing the best performance, for the blue-PAA450/PVB210 electrode, the state of capacity fade is reached after 58 full cycles whereas for the blue-PAA450/PVB60 it is 29 cycles (Figure 4c). The state of capacity fade for pure PAA is 38 cycles, which is slightly higher than for both black compositions (33 cycles for black-PAA/PVB210 and 35 cycles for black-PAA/PVB60).

These results arise two important questions: (**a**) Why does the electrode with the blue-PAA450/PVB210 composition show significantly better performance than the blue-PAA450/PVB60? What else is important in the composition of the PAA/PVB polymer blend for the improved performance of the Si electrode? (**b**) Why does a well-known and a broadly used PAA polymer as a binder for Si-based electrodes perform worse than its equimolar mixture with PVB?

In order to better address these questions, the best performing blue compositions were chosen, and additional electrochemical and physical characterization were performed.

It can been seen in Figures 2c and 3c that the specific capacity values after 100 cycles for the blue compositions are almost the same, i.e. 2167 mAh/g for blue-PAA450/PVB210 and 2121 mAh/g for blue-PAA450/PVB60. However, as shown clearly in Figure 4c, they have principally different capacity fading behavior. To understand these results additional electrochemical measurements on capacity retention under different currents was performed. Figure 5 shows specific lithiation capacities and CE with different current rates after every 12–15 cycles. The capacities are higher for the blue-PAA450/PVB210 at every current rate, and in the case of the blue-PAA450/PVB60 electrode the capacity drops faster with increasing current without stabilization at the end of changed current. Although both electrodes cannot withstand 4 mAh/$g_{(Si)}$, under which the capacity is almost zero, the capacities of two electrodes have more than 500 mAh difference after completing 100 cycles. For the blue-PAA450/PVB210 binder electrode, the capacity recovery, when the current is reduced stepwise, is significantly better than for the blue-PAA450/PVB60, and after 100 cycles it is around 2000 mAh/$g_{(Si)}$, the same as after cycling at a constant current (Figure 3c).

Poor capacity retention results from many factors, where the total resistance of the electrode reflected in the kinetics being a big part. Bad homogeneity of the electrode, i.e. isolated Si, can certainly aggravate that issue. As has been discussed above, the homogeneity of the electrode improves with a higher mass fraction of PVB in the PAA/PVB mixture (Table II, Figures S14-S16). Since there is a higher fraction of PVB210 in the blue-PAA450/PVB210 composition (33 wt%) vs. 10 wt% of PVB60 in blue-PAA450/PVB60, a better electrode homogeneity is expected for the blue-PAA450/PVB210 composition and this may have helped toward a better capacity retention capability of the electrode. High current used in the capacity retention test can also be considered as a test for the mechanical stress on the electrode. Therefore, to shed further light on these results a bulk peeling test was performed on the two electrodes, in order to understand the adhesion to the current collector.

Electrode adhesion to the current collector.—A bulk-scale peeling tests were performed on the electrodes containing pure PAA or PVB polymers and both blue compositions. The results of the tests are plotted in Figure 6. The averaged adhesion to Cu foil of the electrode consisting of pure PAA450 binder was found to be the least (~0.1 N) while the electrodes with both pure PVB60 and PVB210 polymers sustained the maximum force of our experimental setup, i.e. 2.4 N. These results can be expected, since PAA has a highly polar

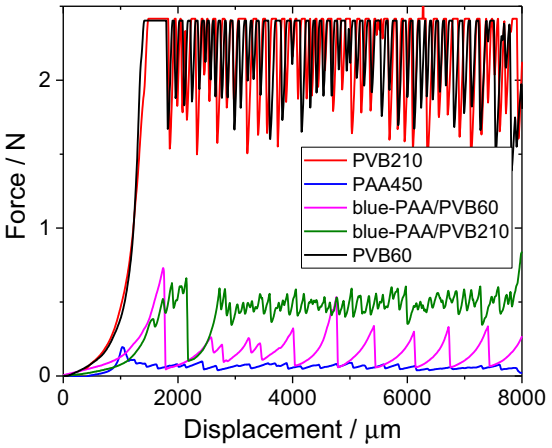

Figure 6. Bulk-scale peeling tests for the electrodes with PAA450 (blue line), PVB60 (black line), PVB210 (red line), blue-PAA450/PVB60 (pink line) and blue-PAA450/PVB210 (green line) compositions.

nature compared to PVB. The averaged peeling force of the electrode coating with the blue-PAA450/PVB210 composition is 0.5 N, which is higher than that for the blue-PAA450/PVB60 electrode. For the blue-PAA450/PVB60 electrode a large variation of peeling force was observed during measurements which appeared as sharp and discrete peaks. This is likely a reflection of the local inhomogeneity of the electrode coating. As there is a lower mass fraction of PVB in blue-PAA450/PVB60, there is more segregation of Si-NPs as it is expected in PAA-rich regions which may lead to large changes in the peeling force as observed, such that the lower end of the force range is in the range of pure PAA. Thus, the peeling force with blue-PAA/PVB compositions lies in between the pristine PAA and PVB electrodes and depends on the weight ratio of less adhesive PAA to more adhesive PVB (Table II).

These results contribute to the answer of the first issue (**a**) raised after analysis of the electrochemical performance. In addition to the inappropriate ratio between the functional groups in the blue-PAA450/PVB60 composition, which may hinder the formation of a dense polymer network, low adhesion and thus potential loss of contact with Cu-foil are the reasons for its worse performance.

We believe that these measurements also help in answering question (b): due to a significantly better adhesion to the Cu-foil, the electrode with blue-PAA450/PVB210 shows a better performance than the electrode containing pure PAA. The bad homogeneity of the PAA-electrode (Figure S14-S16) can facilitate the delamination process. Moreover, due to local inhomogeneities, the capacity fade in blue-PAA450/PVB60 is similar to that observed in PAA, even though the blue-PAA450/PVB60 electrode shows better specific capacity over cycling. Since our electrodes have a mass loading of 1.5–1.8 mg/cm^2, for designing pouch-cells (where the electrode adhesion has much higher priority in comparison to coin or Swagelok cells) and for electrodes with a loading of 5 mg/cm^2 (where the capacity fade due to delamination can be more pronounced) it could be even more crucial to choose an optimal PAA/PVB mixture instead of pure PAA.

Characterization of PAA/PVB polymer mixtures.—The PAA and PVB polymers contain COOH and OH groups, respectively, and there is a possibility of an esterification reaction at elevated temperatures. This in turn may have an effect on the binder performance. The drying conditions used in this work (see Experimental) do not imply an esterification reaction. They are used to get rid of remnant moisture which may affect the battery performance. However, earlier reports, where the same drying conditions have been used for PAA and polyvinyl alcohol (PVA), which contain the carboxylic and hydroxyl functional groups similar to the PAA/PVB system, state that the final PAA/PVA binder possesses covalent ester bonds.[47] Therefore, in order to verify

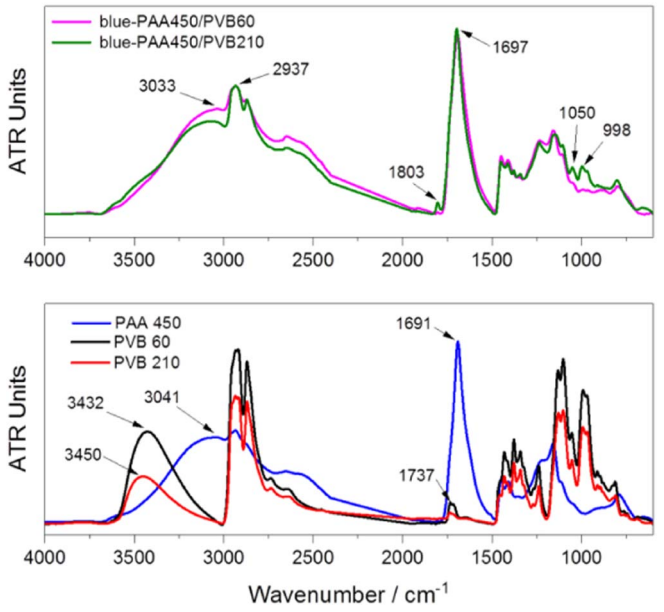

Figure 7. ATR-FTIR spectra of single components (bottom): PAA450 (blue line), PVB60 (black line), PVB210 (red line) and of film polymer mixtures (top): blue-PAA450/PVB60 (pink line) and PAA450/PVB210 (green line) compositions.

the chemical structure, FTIR was conducted on pure PAA and PVB polymers as well as blue-PAA/PVB mixtures. The spectra for all measurements are plotted in Figure 7. In the spectra of the mixtures after drying a weak band at 1802 cm^{-1} is observed which indicates the presence of anhydride (asymmetrical stretching vibration of C=O group; two bands at 1050 and 998 cm^{-1} are corresponding to stretching vibrations of C-O-C and C-O groups in PVB).[35] In the case of esterification, one would expect a shift of the stretching vibration band of C=O group of PAA (from 1697 to ~1730 cm^{-1})[35] to higher wavenumbers or an appearance of a new band at ~1730 cm^{-1}, whereas we observe only a slight shift of the aforementioned band. The ester band may also be disguised by the strong and broad stretching vibration band of C=O group in PAA, and since PVB contains a few wt% of acetate groups (1737 cm^{-1}) initially (Table I) the fact of covalent bonding between PAA and PVB cannot be confirmed by FTIR unambiguously. However, the stretching vibration band of the O-H-bond in PAA is red shifted (from 3041 cm^{-1} for a single component to 3033 cm^{-1} in the mixture; stretching vibration bands of O-H bonds of PVB at ~3450 (PVB 210)/3432 (PVB 60) cm^{-1} are overlapped by the OH-band of PAA) which is a sign of H-bonds existing between PAA and PVB. Hereby, it is assumed that in our electrodes mixed PAA and PVB chains are not "fixed" in their position and should adapt to the volume change of Si-nanoparticles under lithiation/delithiation processes via accommodative H-bonds.

Post mortem SEM analysis.—In order to connect the electrode performance with macroscopic electrode characteristics, we carried out detailed post mortem SEM analysis, where the main goal was to analyze the evolution of electrode thickness and surface morphology after a certain cycling history and relate it to binder properties. For this experiment we took both blue-PAA/PVB composition electrodes as well as the electrodes where PAA450, PVB210 or PVB60 were used as individual binders. In the focus of this analysis were four cycling histories: (i) after the first lithiation; (ii) after the first delithiation, i.e. one complete cycle; (iii) after 10 cycles; (iv) after 30 cycles. As a reference the properties of the pristine electrode with the corresponding binder were considered.

SEM micrographs made from electrode surfaces with low magnification are shown in Figure 8. All five electrodes do not undergo any morphological change after the 1st lithiation, which should be related to the similar density of all electrodes (Table III) and thus similar free space provided by the porosity, necessary for the volume expansion of Si-NPs. It is rather remarkable that after full cycles, i.e. cases (ii), (v) and (iv), the electrodes with pure PVB binders do not show structural disruptions, while the surfaces of electrodes with PAA450 binder and blue-PAA/PVB compositions demonstrate multiple cracks. For the blue-PAA450/PVB210-based electrode, where the distribution of Si and C is slightly better due to a higher wt% of PVB210 (Figures S14-S16), cracking after the first cycle is less pronounced. However, after 30 cycles the morphology of this electrode is similar to that of blue-PAA450/PVB60 and PAA450 electrodes.

A smooth surface of PVB-based electrodes was not caused by a thick SEI layer which may clamp possible clefts. This was confirmed by high magnification SEM images where individual Si-NPs are well recognized for all cases (Figure S17). Similar micro-cracks have been reported for alginate-based electrodes and considered to be a symptom of the stress built in the electrode films.[51] The large volume change of Si is not efficiently compensated due to the stiffness of the alginate binder.[51] Since PAA and alginate have similar mechanical properties,[17,22,41] such a pattern has a similar reason in the case of PAA-based electrodes. We suggest that cracking of PAA- or PAA/PVB-based electrodes is additionally strongly effected by inhomogeneous distributions of Si and CB components as seen in BSE images (Figures S14-S16). Due to these inhomogeneities, the volume decrease during the delithiation process can lead to a stronger electrode disintegration and final cracking. If the electrode coating in the pristine state has a low adhesion to Cu-foil, this rupture promotes the failure of the electrode. The higher the number of cracks (formation of small islands between those cracks), the easier the delamination of the electrode coating from the current collector.

Cracking and delamination turn out to be the main obstacles of getting reliable results from the analysis of the electrode thickness evolution with different cycling histories. Figure 9 shows two representative examples of samples where the surface morphology shows completely different degrees of integrities: SEM-images of PVB60- and PAA450-electrode cross-sections after 30 cycles are compared. In the case of PVB60-electrode, the preserved integrated surface morphology is easily visible in Figure 8 and it enables us to make ~300 μm long cut with an uniform electrode coating, such that the thickness can be determined with a small deviation. On the other hand, the PAA450-electrode is the most problematic in its handling because of the multiple cracking and ease of delamination which is traced back to its low adhesion to Cu (Figure 6). After just 1 cycle, only a small electrode area of ~140 μm could be cut without embedding into epoxy resin (Figure S18). Moreover, as the obtainable uniform cut area gets smaller, estimation of the electrode thickness becomes less reliable.

The PAA450-electrode sample was then fixed in epoxy glue and cut. The SEM examination reveals a non-uniform thickness of the coating with thinner (39 μm) and thicker areas (50 μm) which can be an indication of different degree of lithiation/delithiation due to delamination (Figure 9). An absence of an abrupt capacity drop while cycling the PAA450-electrode (Figures 2c and 3c) indicates that the fully peeled electrode areas on SEM-image of Figure 9b are a result of sample preparation. This means that the averaged electrode thickness derived from a particular areal cut would not necessarily coincide with the one derived from a cut made a few mm aside. In order to define the desired characteristic a serial study has to be done, where a dozen of cross-sections should be analyzed using statistical tools. In our study we demonstrate the problematic issue of such analysis and emphasize the challenges thereof.

Changes of electrode thicknesses after different cycling histories are summarized in Table IV. Due to reliability of the thickness measurements outlined above, the values are considered only qualitatively. Each number is an averaged value calculated from one or two 140–550 μm long cross-sections similar to those shown in Figure 9 and Figure S18. The SEM-micrographs given in Figure S19 represent the cross sections of all electrodes at a higher magnification. The delamination from Cu-foil is a common feature of cycled

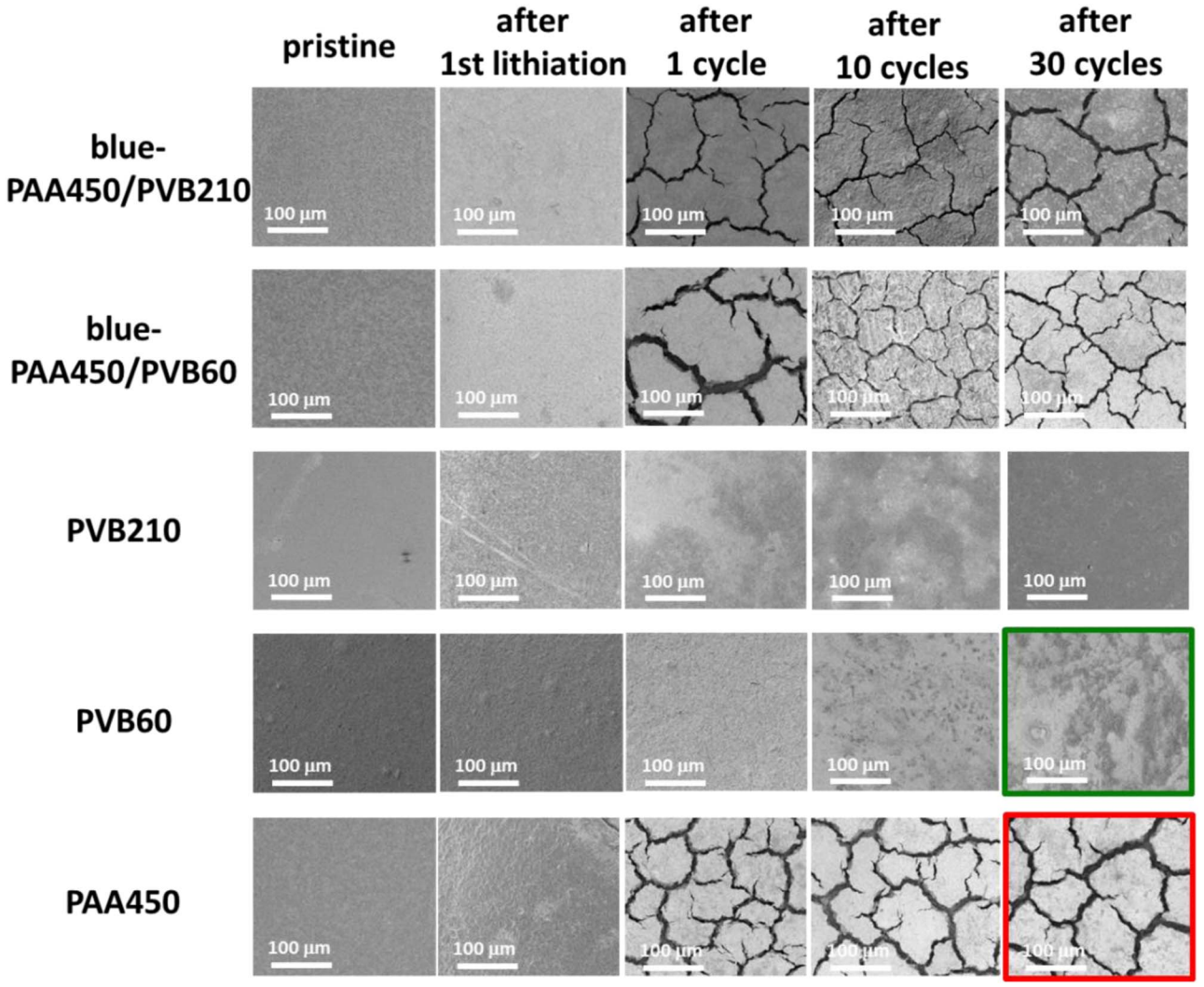

Figure 8. Surface morphology of silicon electrodes before and after cycling using different binders. All SEM micrographs (InLens detector) are made at the same magnification. Green and red frame indicate samples for which SEM of cross sections are given in Figure 9.

electrodes and only for PVB-containing electrodes it is less frequently observed, which is related to the higher adhesion of the pristine electrodes with PVB-binders to Cu (Figure 6). As one would expect from the binder mechanical properties (Figure 1), the electrodes with pure soft PVB binders expand stronger, i.e. to ∼160 %, after the first lithiation, compared to the PAA450- and PAA/PVB- electrodes (Table IV). The expansion of both blue-PAA/PVB electrodes is less than the one of the pure PAA electrode. We suggest that this is related to the synergetic effect of PAA and PVB polymer chains that can preserve the electrode integrity under volume expansion, thus forming a polymer network. PAA makes a mechanically stiff polymer "scaffold" which adheres stronger to the native oxide layer of Si-NPs but has a lower adhesion to CB particles due to its polar nature, leading to segregation of Si-NPs. Addition of PVB forms an additional network,

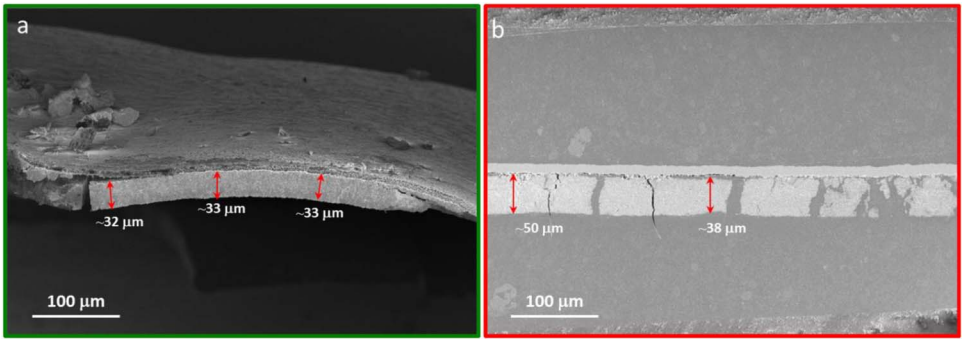

Figure 9. SEM-images (InLens detector) of cross-sections after 30 cycles (a) PVB60-electrode and (b) PAA450-electrode embedded in epoxy resin. Both SEM micrographs (InLens detector) are made at the same magnification.

Table IV. Summary of the change of electrode thicknesses after cycling using different binders as obtained from the post mortem SEM analysis.

Binder composition	Electrode expansion (%)			
	After 1st lithiation	After 1 cycle	After 10 cycles	After 30 cycles
blu-PAA450/PVB210	135 (±20)	117 (±18)	134 (±18)	187 (±22)
blue-PAA450/PVB60	134 (±18)	122 (±28)	142 (±23)	174 (±19)
PVB210	163 (±15)	114 (±16)	124 (±15)	138 (±17)
PVB60	161 (±16)	112 (±14)	134 (±16)	143 (±13)
PAA450	146 (±18)	108 (±24)	131 (±25)	179 (±23)

with a good adhesion to Si-NPs and PAA via H-bonding and to CB via Van der Waals forces, as well as to Cu-foil. The optimal PAA/PVB blend thus has good adhesion as well as good mechanical properties. The H-bonding between polymers and Si-NPs was confirmed through ATR-FTIR measurement of one of the PAA/PVB mixtures and pure Si-NPs (see Figure S21).

After 1 and 10 cycles the electrode expansion values are scattered at around 115% and 133%, respectively. A qualitative difference can be seen after 30 cycles, where both electrodes containing pure PVB have the lowest expansion of ∼138-143% versus ∼174-187% of PAA450 and both PAA/PVB electrodes (Table IV). As observed in the electrochemical cycling data, the capacity fading for the electrodes with PVB210 or PVB60 is most significant and there is over 75% capacity loss after 30 cycles (Figures 2c and 3c). The best performing blue-PAA450/PVB210-electrode expands the most after 30 cycles, i.e. ∼187%, however its value does not differ significantly from the pure PAA450 electrode and blue-PAA450/PVB60 electrode, where the averaged expansion values are ∼174% and ∼179%, respectively. We suppose that repeated expansion of Si-particles alters the binder properties and its ability to preserve the integrity weakens during cycling, which is reflected in similar expansion values (Table IV). Accordingly to this assumption, the low expansion of ∼138% and ∼143% of PVB-electrodes can be explained by faster altering of PVB.

Conclusions

In summary, we have characterized PVB for the first time as a binder for Si nanoparticle-based electrodes for application in LIBs. The binder properties such as swelling behavior, Young's modulus and adhesion strength were determined by AFM and compared to the same characteristics of PAA. Since PVB contains non-polar butyral groups and polar hydroxy groups, the prepared Si-electrodes demonstrate a much better homogeneity of Si and CB components. However, the non-polar nature of PVB leads to undesired swelling in the electrolyte solvent which decreases the Young's Modulus. Thus, the study of PVB polymers as individual binders demonstrated worse performance as compared to pure PAA as a binder, which is understood to be a result of impaired mechanical properties in the electrolyte solvent.

Since COOH groups of PAA and OH groups of PVB can form H-bonds, PAA/PVB mixtures have been analyzed as two component binders to form a polymer network where the properties of both shall be combined. A systematic investigation of six PAA/PVB mixtures revealed that one of the key criteria for an improved electrochemical performance of Si-electrodes is an equal molar ratio of polymers as well as a close to equal ratio of COOH to OH groups. The mass percentage of the PVB component (10 wt% vs. 33 wt%) in PAA/PVB mixture also plays an important role with respect to an adhesion improvement of the electrode coating on Cu-foil and a better mixing of Si with CB particles. After 100 cycles specific capacities as high as 2170 mAh/g of electrodes with a Si loading of ∼1 mg/cm^2 were achieved for the PAA/PVB-based electrodes. Post mortem SEM analysis of both the electrode surface and the cross-sections revealed a reduced disintegration of PAA/PVB-based electrodes, which is assigned to the presence of PVB, which forms a flexible polymer network additional to the stiff PAA net present in the electrode structure.

These results are important because of the necessity of novel binders for Si-based electrodes which should enable a preparation of electrodes with high mass loading e.g. 5 mg/cm^2 combined with a non-toxic solvent and a simple preparation technique. The present work is the first complex study on PAA/PVB binders. In order to fully understand the potential of this system to improve capacity retention additional PAA/PVB combinations have to be studied. However, the presented results allow to derive algorithms for polymer compositions that are promising to improve the electrode performance further, thus reducing the sampling in future experiments. For example, the combination of high molecular PVB with PAA of the same M_w may lead to both an efficient PAA/PVB polymer network and an improved adhesion to Cu. Because PAA and PVB are commercially available and cost-efficient they fulfil the basic requirements of an industrial application. The advantages of this new binder will become apparent especially in pouch cells where no pressure is applied on the electrode stack during cycling whereby the adhesion to Cu-foil is of much higher concern.

Acknowledgments

The authors thank Kerstin Arnhold for TGA measurements, Michael Göbel for valuable support in taking high resolution SEM images, Petr Formánek for TEM and Anne Baasner for organizing the bulk peeling test. We gratefully acknowledge funding from the German Federal Ministry of Education and Research (BMBF) through the Excellent Battery – WING center "Batteries – Mobility in Saxony" (grant No. 03X4637C, 03X4637D).

ORCID

Anna Urbanski https://orcid.org/0000-0002-1748-5345

References

1. J. M. Tarascon and M. Armand, "Issues and challenges facing rechargeable lithium batteries," *Nature*, **414**, 359 (2001).
2. J. W. Choi and D. Aurbach, "Promise and reality of post-lithium-ion batteries with high energy densities," *Nat. Rev. Mater.*, **1**, 16013 (2016).
3. C.-Y. Wang, T. Xu, S. Ge, G. Zhang, X.-G. Yang, and Y. Ji, "A Fast Rechargeable Lithium-Ion Battery at Subfreezing Temperatures," *J. Electrochem. Soc.*, **163**, A1944 (2016).
4. J. Janek and W. G. Zeier, "A solid future for battery development," *Nat. Energy*, **1**, 16141 (2016).
5. L. Christensen and M. N. Obrovac, "Structural Changes in Silicon Anodes during Lithium Insertion/Extraction," *Electrochem. Solid-State Lett.*, **7**, A93 (2004).
6. H. Wu and Y. Cui, "Designing nanostructured Si anodes for high energy lithium ion batteries," *Nano Today*, **7**, 414 (2012).
7. U. Kasavajjula, C. Wang, and A. Appleby, "Nano- and bulk-silicon-based insertion anodes for lithium-ion secondary cells," *J. Power Sources*, **163**, 1003 (2007).
8. S. C. Jung, J. W. Choi, and Y.-K. Han, "Anisotropic Volume Expansion of Crystalline Silicon during Electrochemical Lithium Insertion: An Atomic Level Rationale," *Nano Lett.*, **12**, 5342 (2012).
9. Y. Sun, N. Liu, and Y. Cui, "Promises and challenges of nanomaterials for lithium-based rechargeable batteries," *Nat. Energy*, **1**, 16071 (2016).
10. T. Shen, Z. Yao, X. Xia, X. Wang, C. Gu, and J. Tu, "Rationally Designed Silicon Nanostructures as Anode Material for Lithium-ion Batteries," *Adv. Eng. Mater.*, **20**, 1700591 (2018).
11. J.-Y. Li, Q. Xu, G. Li, Y.-X. Yin, L.-J. Wan, and Y.-G. Guo, "Research progress regarding Si-based anode materials toward practical application in high energy density Li-ion batteries," *Mater. Chem. Front.*, **1**, 1691 (2017).

12. J. K. Lee, C. Oh, N. Kim, J.-Y. Hwang, and Y.-K. Sun, "Rational design of silicon-based composites for high-energy storage devices," *J. Mater. Chem. A*, **4**, 5366 (2016).
13. D. Mazouzi, Z. Karkar, C. Hernandez, J. Manero, D. Guyomard, L. Roué, and B. Lestriez, "Critical roles of binders and formulation at multiscales of silicon-based composite electrodes," *J. Power Sources*, **280**, 533 (2015).
14. N.-S. Choi, S.-Y. Ha, Y. Lee, J. Y. Jang, M.-H. Jeong, W. C. Shin, and M. Ue, "Recent Progress on Polymeric Binders for Silicon Anodes in Lithium-Ion Batteries," *J. Electrochem. Sci. Technol.*, **6**, 34 (2015).
15. H. Zhao, W. Yuan, and G. Liu, "Hierarchical electrode design of high-capacity alloy nanomaterials for lithium-ion batteries," *Nano Today*, **10**, 193 (2015).
16. R. R. Garsuch, D.-B. Le, A. Garsuch, J. Li, S. Wang, A. Farooq, and J. R. Dahn, "Studies of Lithium-Exchanged Nafion as an Electrode Binder for Alloy Negatives in Lithium-Ion Batteries," *J. Electrochem. Soc.*, **155**, A721 (2008).
17. A. Magasinski, B. Zdyrko, I. Kovalenko, B. Hertzberg, R. Burtovyy, C. F. Huebner, T. Fuller, I. Luzinov, and G. Yushin, "Toward Efficient Binders for Li-Ion Battery Si-Based Anodes: Polyacrylic Acid," *ACS Appl. Mater. Interfaces*, **2**, 3004 (2010).
18. J. S. Kim, W. Choi, K. Y. Cho, D. Byun, J. Lim, and J. K. Lee, "Effect of Polyimide Binder on Electrochemical Characteristics of Surface-Modified Silicon Anode for Lithium Ion Batteries," *J. Power Sources*, **244**, 521 (2013).
19. Y. K. Jeong, T.-w. Kwon, I Lee, T.-S Kim, A. Coskun, and J. W. Choi, "Hyper-branched β-Cyclodextrin Polymer as an Effective Multidimensional Binder for Silicon Anodes in Lithium Rechargeable Batteries," *Nano Lett.*, **14**, 864 (2014).
20. H. Buqa, M. Holzapfel, F. Krumeich, C. Veit, and P. NovaŕFk, "Study of Styrene Butadiene Rubber and Sodium Methyl Cellulose as Binder for Negative Electrodes in Lithium-Ion Batteries," *J. Power Sources*, **161**, 617 (2006).
21. N.-S. Choi, K. H. Yew, W.-U. Choi, and S.-S. Kim, "Enhanced Electrochemical Properties of a Si-Based Anode Using an Electrochemically Active Polyamide Imide Binder," *J. Power Sources*, **177**, 590 (2008).
22. I. Kovalenko, B. Zdyrko, A. Magasinski, B. Hertzberg, Z. Milicev, R. Burtovyy, I. Luzinov, and G. Yushin, "A Major Constituent of Brown Algae for use in High-Capacity Li-Ion Batteries," *Science*, **334**, 75 (2011).
23. T.-W. Kwon, J. W. Choi, and A. Coskun, "The emerging era of supramolecular polymeric binders in silicon anodes," *Chem. Soc. Rev.*, **47**, 2145 (2018).
24. M. Wu, X. Xiao, N. Vukmirovic, S. Xun, K. Das, X. Song, P. Olaide-Velasco, D. Wang, A. Z. Weber, L.-W. Wang, V. S. Battaglia, W. Yang, and G. Liu, "Toward an Ideal Polymer Binder Design for High-Capacity Battery," *J. Am. Chem. Soc.*, **135**, 12048 (2013).
25. C. Erk, T. Brezesinski, H. Sommer, R. Schneider, and J. Janek, "Toward Silicon Anodes for Next-Generation Lithium Ion Batteries: A Comparative Performance Study of Various Polymer Binders and Silicon Nanopowders," *ACS Appl. Mater. Interfaces*, **5**, 7299 (2013).
26. U. S. Vogl, K. Das, A. Z. Weber, M. Winter, R. Kostecki, and S. F. Lux, "Mechanism of Interactions between CMC Binder and Si Single Crystal Facets," *Langmuir*, **30**, 10299 (2014).
27. I. Cho, S. Gong, D. Song, Y.-G. Lee, M.-H. Ryou, and Y. M. Lee, "Mussel-inspired Polydopamine treated Copper Foil as a Current Collector for High-performance Silicon Anodes," *Sci. Rep.*, **6**, 30945 (2016).
28. X. Zhang, H. Hao, Y. Shi, and J. Cui, "The mechanical properties of Polyvinyl Butyral (PVB) at high strain rates," *Constr. Build. Mater.* **93**, 404 (2015).
29. U. Keller and H. Mortelmans, "Adhesion in Laminated Safety Glass - What makes it work?," *Glass Processing Days, Conference Proceedings - 6th International Conference on Architectural and Automotive Glass 13.-16.06.1999*, Tampere, Finland, 353–356 (1999).
30. C. Fors, Mechanical properties of interlayers in laminated glass. Experimental and Numerical Evaluation, Master's Dissertation, Lund University (2014).
31. F. Lian, Y. Wen, Y. Ren, and H.-Y. Guan, "A novel PVB based polymer membrane and its application in gel polymer electrolytes for lithium-ion batteries," *J. Membr. Sci.*, **456**, 42 (2014).
32. D. Shirley, "High-resolution X-ray photoemission spectrum of the valence bands of gold," *Phys. Rev. B*, **5**, 4709 (1972).
33. I. Luzinov, D. Julthongpiput, P. D. Bloom, V. V. Sheares, and V. V. Tsukruk, "Bilayer nanocomposite molecular coatings from elastomeric/rigid polymers: Fabrication, morphology, and micromechanical properties," *Macro Sym*, **167**, 227 (2001).
34. H. Zhao, Y. Wei, R. Qiao, C. Zhu, Z. Zheng, M. Ling, Z. Jia, Y. Bai, Y. Fu, J. Lei, X. Song, V. S. Battaglia, W. Yang, P. B. Messersmith, and G. Liu, "Conductive polymer Binder for High-Tap-Density Nanosilicon Material for Lithium-Ion Battery Negative Electrode Application," *Nano Lett.*, **15**, 7927 (2015).
35. G. Socrates, *Infrared and Raman Characteristic Group Frequencies. Tables and charts*, 3rd Ed., John Wiley & Sons Ltd., Chichester (2001).
36. J. Dechant, "*Ultrarotspektroskopische Untersuchungen an Polymeren*," Akademie-Verlag, Berlin (1972).
37. C. C. Nguyen, T. Yoon, D. M. Seo, Guduru, and B. L. Lucht, "Systematic Investigation of Binder for Silicon Anodes: Interactions of Binder with Silicon Particles and Electrolytes and Effects of Binders on Solid Electrolyte Interphase Formation," *ACS Appl. Mater. Interfaces*, **8**, 12211 (2016).
38. T. Jaumann, J. Balach, M. Klose, S. Oswald, U. Langklotz, A. Michaelis, J. Eckert, and L. Giebeler, "SEI-component formation on sub-5 nm sized silicon nanoparticles in Li-ion batteries: the role of electrode preparation, FEC addition and binders," *Phys. Chem. Chem. Phys.*, **17**, 24956 (2015).
39. J. Liu, Q. Zhang, T. Zhang, J.-T. Li, L. Huang, and S.-G. Sun, "A Robust Ion-Conductive Biopolymer as a Binder for Si Anodes of Lithium-Ion Batteries," *Adv. Funct. Mater.*, **25**, 3599 (2015).
40. T. Niratiwongkorn, G. E. Luckachan, and V. Mittal, "Self-healing protective coatings of polyvinyl butyral/polypyrrole-carbon black composite on carbon steel," *RSC Adv.*, **6**, 43237 (2016).
41. X.-D. Fan, Y.-L. Hsieh, J. M. Krochta, and M. J. Kurth, "Study on molecular interaction behavior, and thermal and mechanical properties of polyacrylic acid and lactose blends," *J. Appl. Polym. Sci.*, **82**, 1921 (2001).
42. Y. Jin, B. Zhu, Z. Lu, N. Liu, and J. Zhu, "Challenges and Recent Progress in the Development of Si Anodes for Lithium-Ion Battery," *Adv. Energy Mater.*, **7**, 1700715 (2017).
43. H. Zhao, Y. Wei, C. Wang, R. Qiao, W. Yang, P. B. Messersmith, and G. Liu, "Mussel-Inspired Conductive Polymer Binder for Si-Alloy Anode in Lithium-Ion Batteries," *ACS Appl. Mater. Interfaces*, **10**, 5440 (2018).
44. T. M. Higgins, S.-H. Park, P. J. King, C. J. Zhang, N. McEvoy, N. C. Berner, D. Daly, A. Shmeliov, U. Khan, G. Duesberg, V. Nicolosi, and J. N. Coleman, "A Commercial Conducting Polymer as Both Binder and Conductive Additive for Silicon Nanoparticle-Based Lithium-Ion Battery Negative Electrodes", *ACS Nano*, **10**, 3702 (2016).
45. V. L. Chevrier and J. R. Dahn, "First Principles Model of Amorphous Silicon Lithiation," *J. Electrochem. Soc.*, **156**, A454 (2009).
46. C. K. Chan, R. Ruffo, S. S. Hong, R. A. Huggins, and Y. Cui, "Structural and electrochemical study of the reaction of lithium with silicon nanowires," *Journal of Power Sources*, **189**, 34 (2009).
47. J. Song, M. Zhou, R. Yi, T. Xu, M. L. Gordin, D. Tang, Z. Yu, M. Reguly, and D. Wang, "Interpenetrated Gel Polymer Binder for High-Performance," *Adv. Funct. Mater.*, **24**, 5904 (2014).
48. H. Wenzl, "Batteries and fuel cells - Lifetime", in: "*Encyclopedia of Electrochemical Power Sources*", Editor-in-chief: J. Garche, Elsevier, Amsterdam, pp. 552 (2009).
49. E. Talaie, Bonnick, X. Sun, Q. Pang, X. Liang, and L. F. Nazar, "Methods and Protocols for Electrochemical Energy Storage Materials Research," *Chem. Mater.*, **29**, 90 (2017).
50. C. Wang, H. Wu, Z. Chen, M. T. McDowell, Y. Cui, and Z. Bao, "Self-healing chemistry enables the stable operation of silicon microparticle anodes forhigh-energy lithium-ion batteries," *Nat. Chem.*, **5**, 1042 (2013).
51. Y. K. Jeong, T.-W. Kwon, I. Lee, T.-S. Kim, A. Coskun, and J. W. Choi, "Millipede-inspired structural design principle for high performance polysaccharide binders in silicon anodes," *Energy Environ. Sci.*, **8**, 1224, (2015).